Silicon anodes with improved calendar life enabled by multivalent additives

Yunya Zhang[1], * Xiang Li[1], Eric Sivonxay[2], Jianguo Wen[3], Kristin A. Persson[2], John T. Vaughey[1], Baris Key[1], Fulya Dogan[1] *

1. Chemical Sciences and Engineering Division,

Argonne National Laboratory,

Lemont, Illinois 60439, United States

2. Department of Materials Science and Engineering,

University of California,

Berkeley, California 94720, United States

Energy Storage and Distributed Resources Division,

Lawrence Berkeley National Laboratory,

Berkeley, California 94720, United States

3. Center for Nanoscale Materials,

Argonne National Laboratory,

Lemont, Illinois 60439, United States

*Corresponding author. E-mail: yyzhang0601@gmail.com, Tel: 434-282-6262

E-mail: fdogan@anl.gov, Tel: 630-252-1079

Abstract:

Silicon is widely recognized as the most promising upgrade for graphite anodes due to its much higher capacity, natural abundance, and ability to be directly applied in the slurry-based, roll-to-roll production lines. However, in addition to the fast capacity decay, silicon anodes also suffer from inferior calendar life in practical applications due to the unstable solid-electrode interface (SEI). Until now, strategies to effectively improve the calendar life by tailored SEIs remain largely unclear, especially in high-Si content, zero-graphite anodes. Here, silicon anodes with superior calendar life were developed by adding small concentrations of multivalent salts into the baseline electrolyte. The Ca additive reacted with the F ions in the electrolyte, forming a layer of nanocrystalline CaF_2 that was closely coated around the silicon particles. The CaF_2-enabled new SEI was strong and dense, which effectively protected the silicon core from side reactions, leading to lower capacity decay after calendar aging at high voltage. More importantly, the Ca additive was effective universally for all available commercial silicon or SiO sources. This study provides a feasible and low-cost solution for developing silicon anodes with long calendar life, paving the way towards commercially viable silicon anodes.

Graphic abstract:
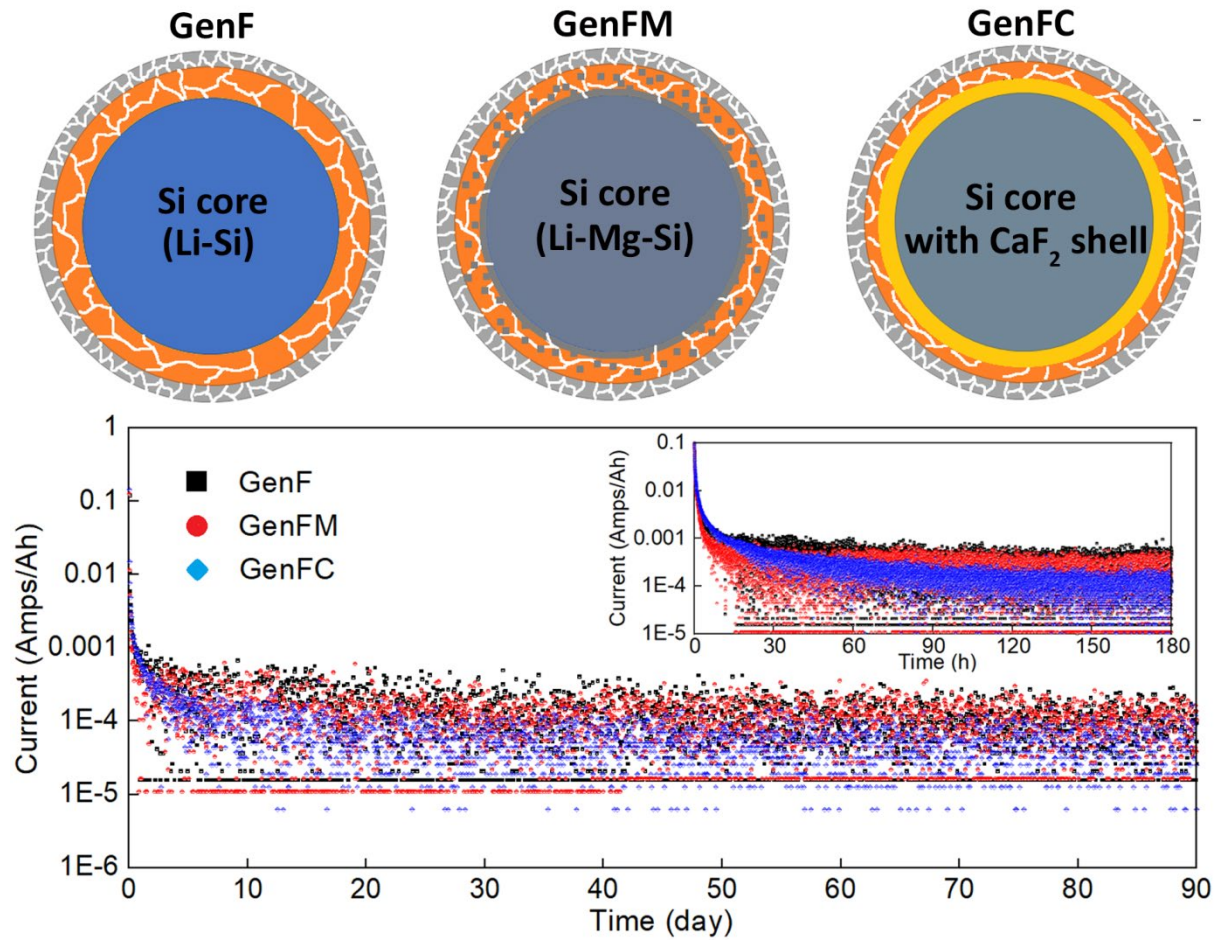
1. Introduction

With the intense increasing demand for sustainable and zero-emission energy consumption, we have witnessed the surge of electric vehicles (EVs) in the past decade.[1] However, concerns over the limited driving range, which is also called 'range anxiety', have become a critical factor that prevented the further promotion of EVs.[2] To improve the energy density of the battery cells, researchers around the world have made significant efforts for developing new cathode materials with higher capacity and higher voltage.[3–5] On the contrary, theoretical modeling indicates that increase the capacity on the anode side is currently a more direct pathway to improve the energy density.[6,7] A promising approach to achieve a notable leap of battery energy is to replace the graphite on the anode side with silicon.[7] With its full lithiated state ($Li_{15}Si_4$), silicon delivers a theoretical capacity of ~3640 mAh/g, approximately 10 times higher than graphite (~370 mAh/g).[8–10] Comparing with another frontrunner high-capacity anode material, Li metal, Si has the advantages of no dendrites or mossy Li formation,[11,12] higher natural abundancy, less restrictive production or storage conditions, and direct applicability in the roll-to-roll production lines designed for graphite electrodes, leading to much better safety and lower cost. However, in practice, these attributes of silicon are offset by issues associated with large volume expansion that occurs with the reversible formation of various lithium silicides (LS) (269.3 % from silicon to $Li_{15}Si_4$), which induce huge stress and strain concentration on the silicon particle, ultimately leading to fracture or pulverization.[13–16] A breakthrough was made when researchers found that the size and structure of the silicon particles are critical for the cyclic

performance of silicon electrodes.[17–19] With a particle size smaller than 100 nm, pulverization due to volumetric change can be largely avoided. Since this discovery, silicon with a variety of nanostructures has been designed and developed,[10,20] including nanoparticles,[21] nanowires,[22] nanotubes,[23] nanofilms,[24,25] hollow nanospheres,[26] and so on. So far, owing to the synergistic contributions from advancements in silicon morphology, electrolytes, and binders, the performance of long cycling life with high capacity retention rate has been achieved in many studies.[27,28]

However, calendar life, another essential property that is particularly important for real-life application,[29] has long been under-studied when compared with the cycling performance in silicon anodes.[30] According to USABC, for a long-life EV, a calendar life of 5 years is desirable.[31] Unlike cycling, which involves volume change and repeated formation of a new solid-electrolyte interface (SEI), calendar life is more related to the stability of the existing SEI and the underlying core. Unfortunately, the SEI of silicon electrodes is notoriously unstable due to the high reactivity of charged Si_2^{-2} and/or Si^{-4} anions that react to reduce the binders and electrolyte components.[32–34] Although the formation, structure, component, and modification of SEI have been studied in detail,[35–38] only a few pieces of literature have reported the calendar life of silicon electrodes. For instance, Abraham *et al.* compared the difference between calendar aging and cycle-life aging in silicon-graphite composite electrodes,[39] Jossen *et al.* discussed the calendar aging of 18650 nickel-rich, silicon-graphite lithium-ion cells,[40] and Jansen *et al.* studied the calendar life of SiO

anodes.[41] However, within the limited literature there was no definite estimation of Si anode calendar life due to the lack of clear understanding of optimum SEI composition and morphology to resist calendar aging and a practical test protocol that can project calendar life effectively. A rough estimation is that most of the Si anodes so far have a calendar life lower than one year, which presents a huge technical gap for qualified EV batteries.[30] Clearly, to effectively improve the calendar life of silicon anodes remains a huge barrier. Based on the current knowledge and technology, Johnson et $al.$ proposed potential strategies to mitigate the capacity decay during calendar aging in their perspective,[30] showing that the key to constructing a system with improved calendar life is to reduce the contact between active Si surface and electrolyte, such as creating molecular surface coatings, building physical shields, and increasing the particles size. Recently, Han et $al.$ used multivalent salts as additives (including $Mg(TFSI)_2$, $Ca(TFSI)_2$, $Zn(TFSI)_2$ and $Al(TFSI)_3$) into the EC+EMC+FEC+ LiPF$_6$ (Gen2+ FEC=GenF) baseline electrolyte, inspired by the improved thermodynamic stability of the fully reduced lithium silicide compounds after Mg, Zn, or Al substitution,[42–44] it was found that the multivalent ions formed Li-M-Si (M=Mg, Ca, Zn, and Al) ternary Zintl phases during electrochemical lithiation. The Zintl phases enhanced the lithiation/delithiation stability and reduced area specific impedance of the negative electrodes, leading to a notable improvement in cycling performance. As a new area in the silicon electrode arena, it is worthwhile to dig deeper and unveil the impacts of multivalent additives on the SEI composition and the calendar life of silicon electrodes in full cells.

Here, $Mg(TFSI)_2$ and $Ca(TFSI)_2$ salts were added to the baseline GenF electrolyte. The full cells with Ca additive exhibited a universal improvement of calendar life performance regardless of silicon sources and cathode materials. For typical Si/NMC532 cells, ones with Ca additive only exhibited a 9.5% capacity loss after three-month calendar aging at high voltage (4.1 V). By combining electrochemical impedance spectroscopy (EIS), transmission electron microscopy (TEM), and magic angle spinning nuclear magnetic resonance (MAS NMR) spectroscopy, it was found that a robust and nonporous coating layer, mainly consisting of CaF_2, formed around the silicon particles when cycled with Ca additive. The enhanced SEI largely improved the silicon electrode's ability to resist calendar aging. This study unveiled that, a strong and nonporous SEI, which can be achieved by electrolyte additives, is the key to protect the silicon from side reactions and prolong the calendar life. As one of the very first studies that study the calendar life of Si anodes from the materials perspective, the study is not only providing new inspirations for SEI design, but also opens a new pathway towards practically usable silicon electrodes for EVs.

2. Results

2.1 Calendar life performance of full cells with different electrolytes.

Graphite-free Si anodes containing 60 wt. % commercial silicon powders from different companies were assembled with NMC532 or LFP cathodes from Argonne's Cell Analysis, Modeling, and Prototyping (CAMP) facility. Three electrolytes, GenF, GenFM, and GenFC

(as shown in **Table 1**), were used, where GenF was the baseline electrolyte. For convenience, GenF, GenFM, and GenFC also represent the tested cells in the following illustrations. When cycling at a rate of C/10 for 100 cycles, the GenFC cell exhibited relatively lower initial capacity but better capacity retention compared to the other two cells (**Figure S1**, Supporting Information). On the other hand, the GenFC cell displayed slightly worse but still decent rate performance comparing with GenF and GenFM cells (**Figure S2**). After the current density increased from 0.1 C to 2 C, the capacity retention rate of the GenFC cell was 67.9 %.

Table 1. Formulations and notations of the electrolytes used in this study

Electrolyte	Formulations
Gen2	1.2 M LiPF$_6$ in a 3:7 mixture of EC and EMC
GenF (baseline)	Gen2 electrolyte + 10 wt% FEC
GenFM	GenF electrolyte + 0.1 M Mg(TFSI)$_2$
GenFC	GenF electrolyte + 0.1 M Ca(TFSI)$_2$

The calendar life test protocol is shown in **Figure 1a**.[45] Specifically, a one-month or three-month holding at high voltage (4.1 V for NMC532 and 3.35 V for LFP) was carried out after three formation cycles at a C/10 rate. After the calendar aging, there are two diagnostic cycles at a C/10 rate. In order to evaluate the calendar life of a newly assembled battery in a reasonable period of time, the internal leakage current at the fully charged state is measured. Any current leakage should result from the side reactions between the lithiated silicon anode and the electrolyte or other cell components. Therefore, a battery with long calendar

life should exhibit a lower leakage current while calendar aging. For the Si(Paraclete)/NMC532 full cells during the three-month holding, the current of the GenFC cell was lower and more convergent than the GenF and GenFM cells, indicating that fewer side reaction(s) occurred in the GenFC cell (**Figure 1b**). A similar conclusion can be drawn from the capacity exchange rate profiles (**Figure 1c**), in which the GenFC cell exhibited a lower value than the other two cells. After 10 days of holding, the capacity exchange curve of the GenFC cell was very much flattened, indicative of fewer side reactions. After three-month holding, the capacity exchange (both reversible and irreversible) in the GenFC cell was about 19 %, lower than that of the GenF cell (27.5 %) and the GenFM cell (25%). There are two approaches to identify the irreversible capacity loss during the calendar aging. The first one is to compare the discharge capacity of the third formation cycle and the second diagnostic cycle (red frames in **Figure 1a**). As shown in **Figure 1d**, the GenFC cells exhibited much smaller capacity decay compared to the GenF and GenFM cells after one- or three-month calendar aging although it started with lower capacity. The average capacity decay rate of the GenFC cells after the one-month holding was 4.07 % and 6.98 % after the three-month holding (**Figure 1e**). In contrast, the average capacity decay rate for the GenF cells was 9.09 % and 13.71 %, while the GenFM cells were 9.71 % and 14.86 %, respectively. For the GenFC cells, most of the capacity loss occurred within the first month of holding. In the following two months, only about 2.9 % capacity was lost due to the calendar aging. The faster capacity fading in the first month is probably due to a synergistic effect of SEI pile-up and anode overhang.[46–48] The second method to identify the capacity

9

loss during the calendar aging is to compare the discharge capacity after holding with the sum of the charge and holding capacity, i.e. the coulombic efficiency of the holding cycle. In this regard, the GenFC cells exhibited superior performance compared to the GenF and GenFM cells. The average coulombic efficiency of the GenFC cells after one-month holding was 91.53 %, and it remained 86.54 % after the three-month holding (**Figure 1f**). On the contrary, the coulombic efficiency of the GenF cells was 85.11 % and 77.52 % after one-month and three-month calendar aging, respectively. The coulombic efficiency of the GenFM cell was 83.58 % and 77.15 % after one-month and three-month calendar aging, respectively.
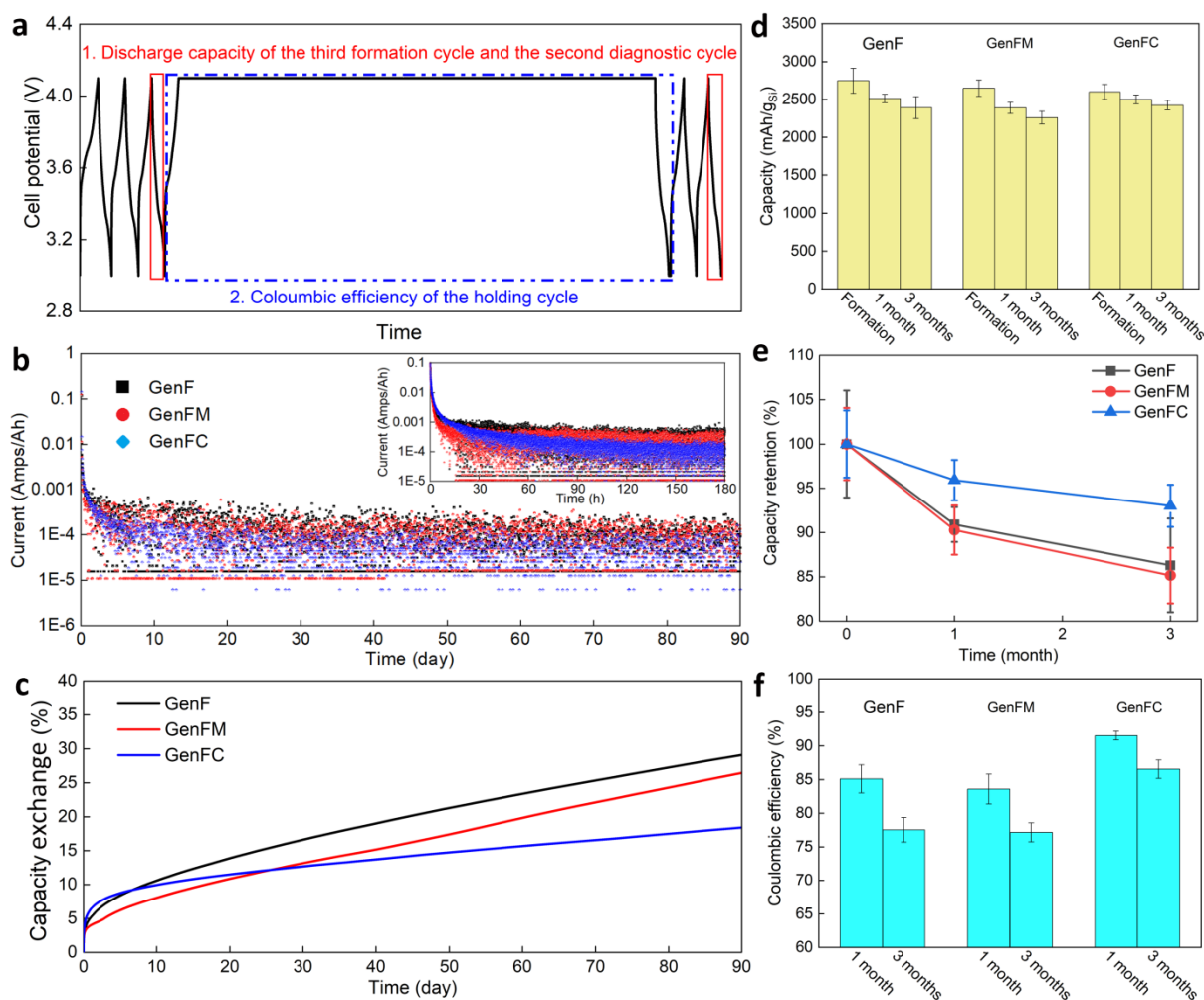
Figure 1. Calendar life of Si/NMC full cells with different electrolytes. a) Calendar life test protocol designed by the U.S. Department of Energy Silicon Consortium Project (SCP). b) Current leakage of GenF, GenFM, and GenFC cells during three-month holding at 4.1 V (1/3000 data points showed) (inset: close inspection of current decay during the first 180 hours (all data points showed)). c) Capacity exchange percentage of GenF, GenFM, and GenFC cells during calendar aging. d) Comparative bar chart of the discharge capacity of the third formation cycle and the second diagnostic cycle. e) Capacity retention rate of the cells after one-month and three-month calendar aging. f) Comparative bar chart of the coulombic efficiency of the holding cycle.

It is important to mention that the role of Ca additive on calendar life is independent of the silicon source and cathode materials. One roadblock on the way of commercialized silicon electrodes is the huge fluctuation of performance due to different electrode preparation methods, surface conditions, and storage approaches, making most of the optimization and

stabilization methods only applicable to certain types of silicon particles. In this study, Ca additives are used for electrodes with silicon from the same manufacturer but different batches (**Figure S3a** and **S3b**), silicon from different companies (**Figure S3c** and **S3d**), SiO (**Figure S3e** and **S3f**), and different cathodes (**Figure S3g** and **S3h**), where all exhibited lower current leakage and capacity exchange during high voltage hold, in comparison to the baseline electrolyte. The holding cycle coulombic efficiency of cells with different silicon sources after one-month holding are compared in **Figure S4**. As expected, the coulombic efficiency of the GenFC cells was higher than the GenF and GenFM cells for all silicon sources. The holding cycle coulombic efficiency of Si/LFP cells after one-month and three-month calendar aging is compared in **Figure S5**. Although the numbers were lower than Si/NMC532 cells in **Figure 1f**, which was due to the insufficient wetting of the thick LFP electrodes required to obtain a similar negative to positive ratio, the coulombic efficiency of the GenFC cells still outperformed the GenF and GenFM cells. Therefore, we conclude that the Ca additive is a potentially universal approach to improve the calendar life of any silicon dominant electrode with different silicon sources in different full cell systems.

2.2 SEM and EDS analysis

In order to understand how Ca additive-enhanced the silicon electrodes show improved calendar life, a series of electrochemical, microstructural, and compositional characterizations were carried out. The SEM image and corresponding EDS element maps of the DMC washed NMC532 cathodes in the Si/NMC532/GenFM and Si/NMC532/GenFC

full cells after one-month calendar aging and the subsequent two diagnostic cycles are shown in **Figure S6**. Unlike O, Ni, Mn, and Co, the distribution of Mg and Ca was homogeneous without apparent preference around NMC particles. The concentration of Mg in the GenFM cell cathode was only 0.18 at. % and the concentration of Ca in the GenFC cell cathode was only 0.14 at. %. Such low concentration is most likely from the residual of salts. On the contrary, the EDS analysis of DMC washed silicon anodes in the GenFM and GenFC cells exhibited a much higher concentration of Mg and Ca with 2.9 at. % and 2.6 at. % (**Figure S7**), more than 10 times higher than observed for the cathodes. Previously, we carried out EDS analysis under TEM on the cathode core after 270 cycles, showing almost no multivalent ions in the cathode materials.[44] The EDS investigations indicate that most of the multivalent ions remained on the anode side and reacted with silicon particles instead of intercalating into cathode materials or contributing to the cathode-electrolyte interfaces (CEIs). This suggests that improved calendar life is due to the new silicon surface layer formed by the multivalent additives in the electrolyte and independent of the cathode used. The multivalent additives also altered the concentration of carbon and oxygen in the Si electrodes. According to the EDS spectra, the concentration of carbon on the GenF electrode was 52.9 at. % and that of oxygen was 26.7 at. %, which were higher than these in the GenFM (C: 48.6 at. %, O: 19.5 at. %) and GenFC (C: 39.6 at. %, O: 23.8 at. %) electrodes. On the contrary, the concentration of fluorine on the GenFC electrode (9.7 at.%) was much higher than that of the GenF electrode (3.8 at. %). This is most likely due to electrolyte additives affected on the formation of the SEI layer and altered the proportion of

organic and inorganic compounds, which will be discussed in more detail in the following sections.

2.3 EIS analysis

EIS spectra of Si/NMC532 full cells with different electrolytes after formation, one-month holding, and three-month holding are shown in **Figure 2**. The values of open circuit voltage (OCVs) of all cells before EIS tests are listed in **Table S1** and **Table S2**, in which all the NMC/Si full cells had an OCV within 2.950 V to 3.050 V, indicative of almost fully delithiated Si electrodes. In order to make most of the details noticeable, the coordinates of **Figure 2a** and **2b** are adjusted according to the size of the EIS profiles and the coordinates of all GenFC profiles are consistent (**Figure 2c** and **2f**). The intercept between the EIS curve and the Z' axis is the equivalent series resistance, which stems from the electrolyte resistance, the intrinsic resistance of the active material, and the interfacial contact resistance between electrodes and current collectors. This part is noted as R_Ω and is equal to a resistance in the equivalent circuit. The semicircle at the high-frequency regime stems from the impedance of ions passing through the SEI on the anode surface, which can be represented as a resistor and a capacitor in parallel in the equivalent circuit. The resistance part is calculated from the diameter of the semicircle and is marked as R_{SEI}. Another larger yet more irregular semicircle in the intermediate frequency regime is the combination of multiple semicircles, which indicate the impedance of the charges transferring between different interfaces, which are mainly influenced by the different passive deposits on the

14

surface of the electrodes. Similarly, it can be represented as a series of combinations of a resistor and capacitor in the equivalent circuit and the sum of the resistance part is noted as R_{ct}. The combined R_{SEI} and R_{ct} can be treated as the resistance of the chargers passing through all interfaces, which is noted as $R_{interface}$. The straight line at the low-frequency regime is the so-called "Warburg impedance" which derives from an ion diffusion limited process in the electrolyte and is denoted as Z_w. The EIS spectra were fitted using a free software EIS Spectrum Analyser and the accurate values of each resistance are listed in **Table S3**. As shown in **Figure 2a** and **Table S3**, the R_Ω of the GenF cells was about 4 Ω and it was consistent after calendar aging. On the contrary, the $R_{interface}$ increased from 16 Ω to 26.9 Ω after high voltage holding. The EIS spectra of the GenFM cells exhibited similar morphology (**Figure 2b**). The R_Ω was about 4 Ω before and after calendar aging. The $R_{interface}$ increased from about 22.4 Ω to 38.8 Ω after the three-month holding. Within the $R_{interface}$, the charge transfer R_{ct} had a notable increase while the R_{SEI} only increased incrementally. Interestingly, unlike the GenF and GenFM cells, which had an interfacial resistance of tens of ohms, the GenFC cells displayed a huge semicircle at the intermediate frequency, indicative of a large R_{ct} (**Figure 2c**). The R_{ct} in the GenFC cells was in a range of 170 to 210 Ω and was relatively stable before and after calendar aging in terms of value and morphology. Close-up inspection of the high-frequency regime of the EIS shows that the R_{SEI} had a minor increase from 2.3 Ω to 4.2 Ω after three-month calendar aging (**Figure 2d**). This large R_{ct} appeared in all different silicon electrodes with different silicon sources after formation (**Figure 2e**). The carbon-coated silicon had a relatively smaller R_{ct} while the

SiO had a higher R_{ct}. However, they both showed similar semicircle morphology. This large

R_{ct} also occurred in the Si/LFP full cells, indicating it is irrelevant to the cathode choice.

The EIS analysis indicates that the Ca additive may stimulate the formation of an extra SEI

layer around silicon particles, which increased the charge transfer resistance but was stable

during calendar aging. The newly formed SEI, although decreased the initial capacity and

resulted in slightly inferior rate performance (**Figure S1** and **S2**), prevented the silicon core

from the attack of electrolytes during high voltage holding, leading to prolonged calendar

life. The Mg additive, on the other hand, may alter the composition or structure of SEI

slightly, which is suggested by the different morphology of EIS, did not induce such a huge

change of SEI impedance characteristics, leading to a smaller improvement in calendar life
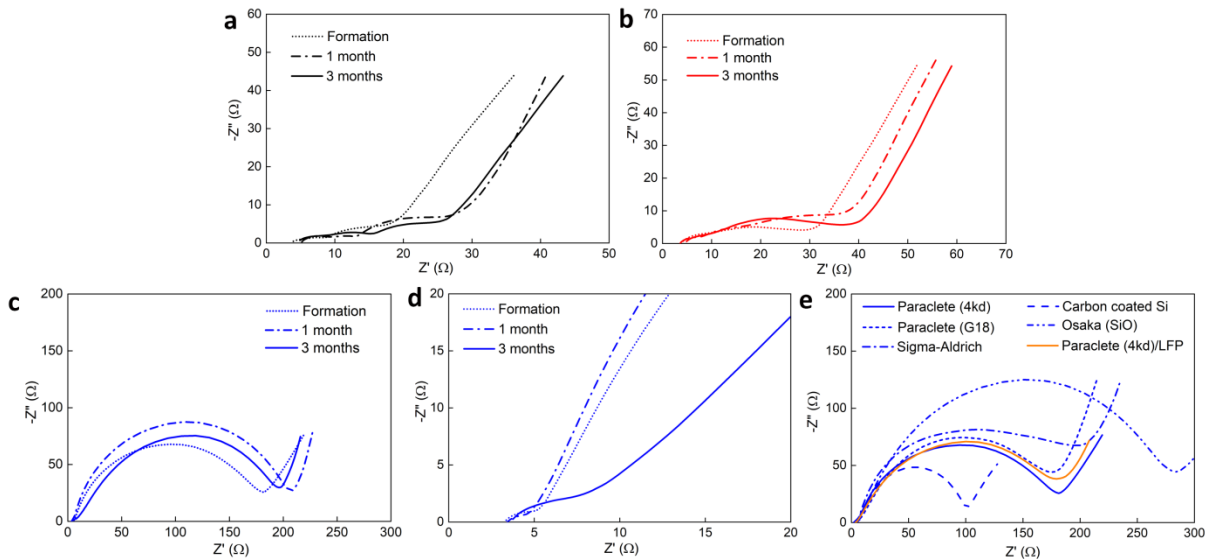
performance compared to GenF cells.

Figure 2. EIS plots of the cells under different conditions. EIS plots of a) GenF b) GenFM c) GenFC cells after formation, one-month holding, and three-month holding. d) Close-up EIS of the GenFC cells at high frequency regime. e) EIS plots of GenFC cells with different silicon sources or cathodes after formation.

2.4 TEM and EDS analysis

To validate the assumption that the Ca additive induced a strong and robust SEI that resisted calendar aging (**Figure 1**) but increased impendence (**Figure 2**), individual silicon particles were observed under a Talos STEM with Super EDS in Argonne Center of Nanoscale Materials (CNM). The high-angle annular dark-field imaging (HADDF) image and energy-dispersive X-ray spectroscopy (EDS) element maps (**Figure 3a** to **3f**) of the silicon particle in a Si/NMC532/GenFC cell after one-month calendar aging exhibited a typical core-shell structure. Surprisingly, the distribution of Ca and F was highly overlapped in the SEI shell (**Figure 3c** and **3d**). EDS line scan (**Figure 3g**) further confirmed this tendency, showing a coating layer consisting of Ca and F with a thickness of 116.9 nm formed around the silicon core. For three silicon particles, the Ca and F layer had an average thickness of 108.7 nm. The bright field TEM image of this silicon particle showed different contrast within the silicon core (**Figure 3h**). The selected area electron diffraction (SAED) pattern revealed that the silicon core had polycrystalline to almost amorphous structure (**Figure 3i**), which was wrapped by a thick SEI shell. The close-up inspection of the shell revealed nanocrystals embedded in an amorphous matrix (**Figure 3j**). SAED pattern in **Figure 3k** suggested that the nanocrystals may be CaF_2. It is worth mentioning that the silicon particle was thoroughly washed by DMC under ultrasonication for three hours before being observed. The SEI with Ca and F, survived such harsh treatment, indicating it was robust and strong. **Figure S8** includes the STEM HADDF image and EDS element maps of a silicon particle in an Si/NMC532/GenFC cell after three-month high voltage holding. The core-shell

structure was retained after the long time of calendar aging (**Figure S8a-S8f**). However, the thickness of the shell reduced to 91.3 nm (**Figure S8g**). According to the inspection of three silicon particles, the average thickness of the SEI layer was 88.7 nm, about 20 nm thinner than that of silicon particles after one-month calendar aging. The thinner CaF_2 layer matches the lower R_{ct} in **Figure 2c**. It is possible that the amorphous, organic matrix that cements CaF_2 nanoparticles may degrade during the long time calendar aging, leading to the falling off of CaF_2 particles.

Interestingly, although the surface of the silicon particle in a Si/NMC532/GenF cell after one-month calendar aging displayed some residual of SEI (**Figure S9a-S9f**), no obvious core-shell structure was noticed. The element distribution, especially F, was inhomogeneous (**Figure S9c**). The EDS line scan profile exhibited no apparent SEI shell around the silicon core (**Figure S9g**), indicating that most of the SEI was removed entirely after DMC washing and ultrasonication. Close-up inspection of the silicon particle surface showed an amorphous structure (**Figure S10a**), which is further validated by the corresponding FFT pattern (**Figure S10b**). The core-shell structure was found in GenFC cells was also not observed for silicon particles in a Si/NMC532/GenFM cell after one-month calendar aging, (**Figure S11a-S11f**). On the surface of the particles, there was a higher concentration of Mg and F (**Figure S11g**). However, the distribution of Mg and F did not overlap, and the Mg rich layer was around 20-30 nm, which is much thinner than that in the Ca layer in GenFC cells. Moreover, the distribution of Mg and Si overlap from the particle edge, indicating Mg

is mostly inserted into the silicon matrix, forming stable Li-Mg-Si ternary Zintl phases. This

is consistent with previous studies,[44] where NMR and HRXRD data showed a higher level

of Mg insertion (approximately 3 times more than Ca) to silicon particles compared to Ca.

Close-up inspection of the silicon particle surface showed a porous morphology with mostly

amorphous structure and sparse nanocrystals (**Figure S12**). This suggests modification of

the SEI morphology and structure around silicon particles are mostly due to the multivalent

additives, especially Ca, providing an improvement in calendar life.
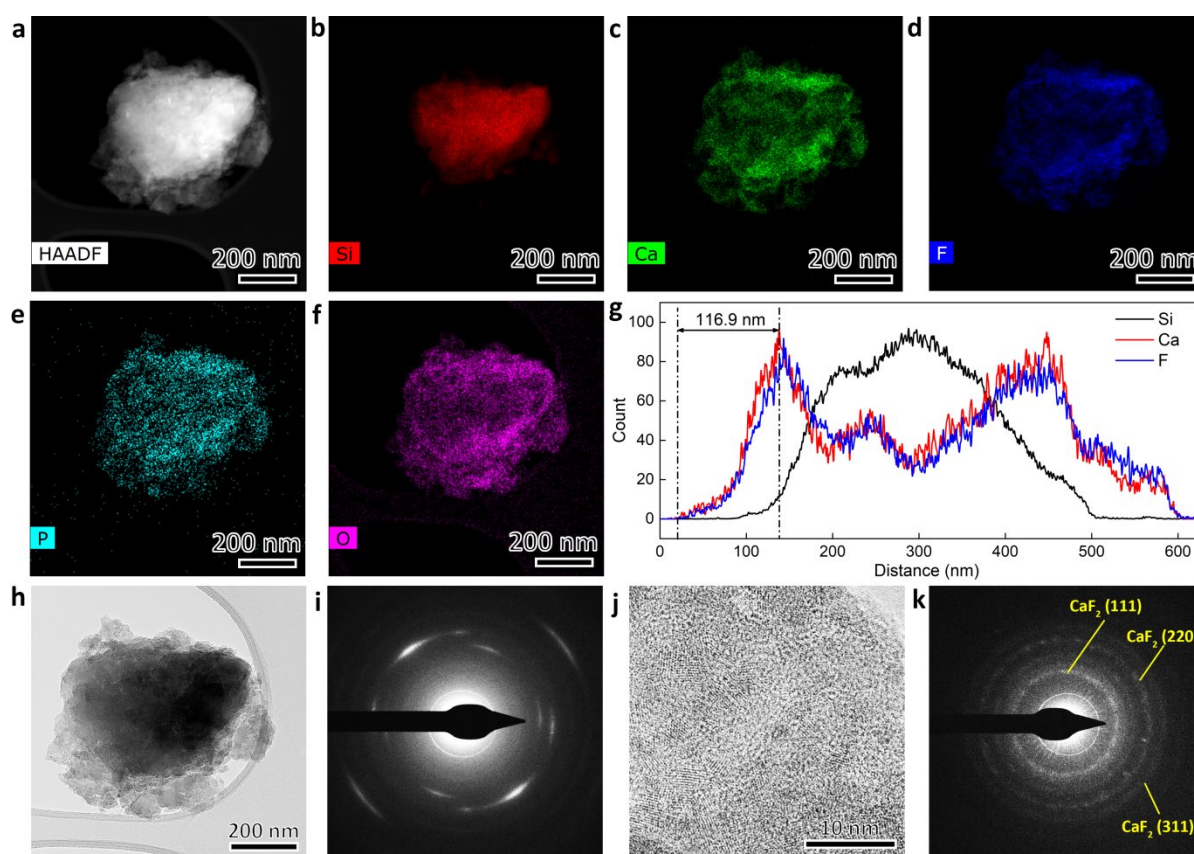
Figure 3. Microstructure and EDS analysis of a silicon particle in a GenFC cell after one-month holding at 4.1 V. a) HAADF image. b) EDS Si map. c) EDS Ca map. d) EDS F map. e) EDS P map. f) EDS O map. g) EDS line scan through the silicon particle, showing that Ca and F are highly aligned. h) TEM bright image of the silicon particle. i) SAED pattern of the silicon core. j) HRTEM of the SEI, showing nanocrystals. k) SAED patter of the nanocrystaline SEI, showing it consists of CaF_2.

2.5 NMR analysis

To further unveil the compositional and structural evolution of the SEIs in Si/NMC full cells with different electrolytes, MAS NMR characterizations were carried out on calendar aged anodes both before and after solvent rinse. The comparison allows us to study both soluble and insoluble SEI species and provides a complementary analysis with the TEM analysis. **Figure 4a** shows the ^{19}F MAS NMR data comparison of silicon electrodes cycled with GenF, GenFM and GenFC electrolyte after one-month calendar aging without DMC rinsing. The major sharp peaks observed around -70ppm in all three electrodes were due to the residual LiPF$_6$ and peaks observed ~ -75 ppm in GenFM, and GenFC samples are due to residual LiTFSI. All three electrodes showed the formation of LiF with a peak ~ -200 ppm and GenFM sample had a shoulder ~ -195 ppm due to MgF$_2$ formation (**Figure 4a inset**). Only GenFC sample had minor peaks at ~ -120 ppm which might be due to FEC polymerization, indicating that the Ca additive may promote the ring-opening reaction of FEC, which would lead to more stable organic species than EC decomposition species. As the salt peaks dominated all the other peaks, it is hard to compare the SEI build-up quantitatively for the three different electrolyte systems. The mass normalized ^{19}F MAS NMR data comparison suggests fluorine bearing SEI species content is higher for GenF than GenFC and GenFM samples. However, the relative intensity of LiF peaks with respect to LiPF$_6$ peaks suggests the LiF build-up after one-month hold was the same for all samples. The possible differences between the organic species composition in SEI for the three

different electrolyte systems were studied by ^{13}C MAS NMR (shown in **Figure 4b**). All three samples had a broad peak at ~ 160 ppm and ~ 25 ppm due to the presence of carboxylate and alky group carbons, respectively. Interestingly, only GenF and GenFM samples had a sharp peak ~ 60 ppm, possibly due to trapped solvent which can be due to excessive build-up of organic SEI observed previously, and is consistent with the more stable nature of the inorganic SEI which may have prevented such build up in GenFC case.[49] This is also consistent with the amount of organic decomposition observed with quantitative ^{13}C MAS NMR (**Figure 4b)** and ^{1}H MAS NMR **(Figure S13**) data comparison, as well as SEM EDS element analysis, suggesting least organic SEI build-up for GenFC and most build-up for GenF. The Si electrodes in GenFC cells after formation, one-month, and three-month calendar aging were further studies with MAS NMR (**Figure 4c**). Apart from the build-up of Li salts, such as LiPF$_6$ and LiF, the peak for CaF$_2$ was also observed at around -100 ppm in one-month and three-month calendar aged samples with Ca additive (**Figure 4c inset**). The nature of insoluble SEI species was also studied by ^{19}F MAS NMR after rinsing the electrodes in DMC. For the GenF electrode, the major ^{19}F NMR peaks were due to LiPF$_6$ decomposition and LiF formation whereas MgF$_2$ and CaF$_2$ were found in the GenFM and GenFC electrodes as major formations, respectively, indicating that the multivalent fluorides are the major inorganic compounds formed with the additives.
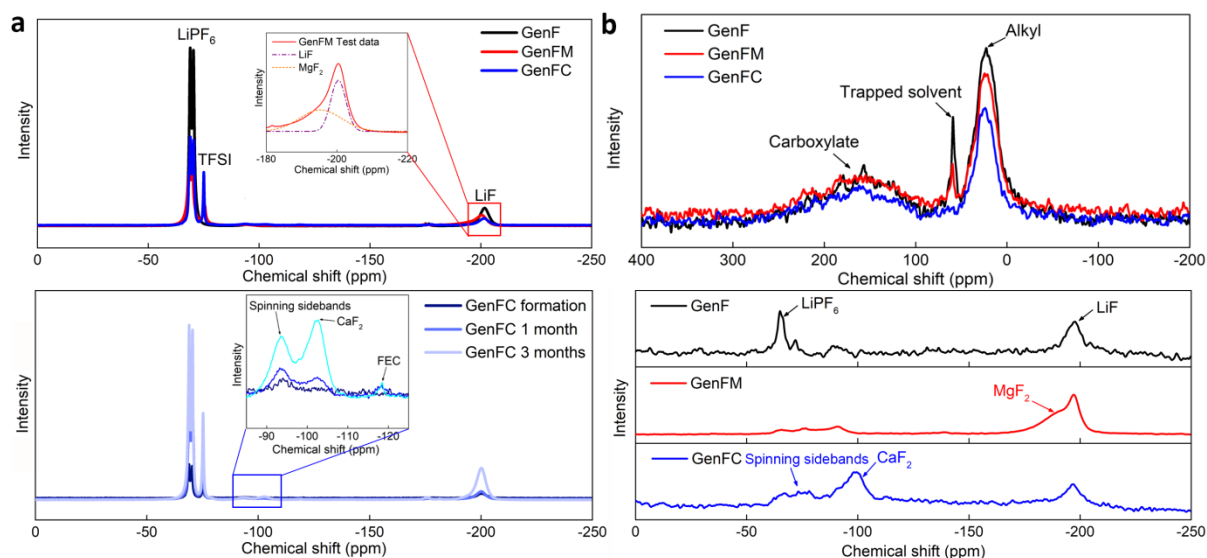
Figure 4. ^{19}F and ^{13}C MAS NMR spectra of delithated silicon. a) ^{19}F NMR spectra of Si electrodes in GenF, GenFM, and GenFC cells after one month of calendar aging and without DMC washing (the intensity is normalized by the weight of the sample). b) ^{13}C NMR spectra of Si electrodes in GenF, GenFM, and GenFC cells after one month of calendar aging and without DMC washing (the intensity is normalized by the weight of the sample). c) ^{19}F NMR spectra of Si electrodes GenFC cells after formation, one month, and three months of calendar aging and without DMC washing (the intensity is normalized by the weight of the sample). d) ^{19}F NMR spectra of Si electrodes in GenF, GenFM, and GenFC cells after one month of calendar aging and with DMC washing.

3. Discussion

It is clear that Ca additive induced the formation of a unique SEI with CaF_2, which is thick and robust enough to survive after ultrasonication and prevents side reactions between Si particles and electrolytes. In order to understand how CaF_2 forms and why the SEI formed with Ca additive is more stable, we identified the possible inorganic compounds that form within the SEI and calculate the formation energies of the most stable polymorphs found in the Materials Project (**Table S4**).[50] According to these first principles density functional theory (DFT) calculations, CaF_2 has the lowest formation energy, indicating that the formation of solid CaF_2 is thermodynamically favorable, i.e. if Ca^{2+} ions from the additive

and F⁻ ions from the decomposition of solvents or salts coexist, the CaF_2 has the highest priority to form. Moreover, the calculated reaction enthalpies for the reactions of Ca with SiO_2, Li_2O, and LiF to form CaO or CaF_2 are all negative, suggesting that Ca can readily replace Si or Li in the oxides or fluorides (**Table S5**). Since the surface of the silicon particles has a conformal native SiO_2 layer and the main inorganic component of the SEI is LiF, they are likely to react with Ca and forming CaO and/or CaF_2. As the compound of the element with the highest electronegativity (F) and a very active alkaline earth metal (Ca), CaF_2 is very stable even in harsh environments,[51] so no further decomposition can occur. Another question is why the Mg additive did not have a notable impact on calendar life. In our previous studies,[44] we showed that Mg ions in the additive diffuse better into the structure, forming the Li-Si-Mg ternary Zintl phases. Contrary to Ca, the ionic radius of Mg is about 35 % smaller. With repetitive lithiation/delithiation, more Mg inserted into the structure and less reacted with surface oxides and electrolyte decomposition products leading to a relatively porous SEI. Moreover, unlike Ca, Mg does not have the ability to modify the SEI by replacing Li in Li_2O or LiF, owing to its positive reaction enthalpies and the tendency to form MgO instead (**Table S5**). Therefore, the Mg additive cannot induce a thick, nonporous, and robust inorganic SEI which can prevent the attack of electrolyte and side reactions.

The combination of TEM and NMR characterizations provides a comprehensive view of the SEI composition and morphology (**Figure 5a**). NMR characterization of washed and

unwashed silicon electrodes provides a better understanding of soluble and insoluble SEI components. For the TEM data, since the sample was ultrasonicated for a long time, it can be assumed that only the strong and robust layer closest to the silicon core survived. Based on the experimental results and previous literature, we can propose the following SEI structures and compositions of the Si particles in the cells with the GenF, GenFM, and GenFC electrolytes. The SEIs around Si particles are often determined by the electrolyte, the Li salt, and the surface condition of Si.[52] According to experimental and calculation results, the SEIs have a multi-layered structure with the outer layer which contains more organic matter and the inner layer which mainly contains inorganic compounds.[53] For the GenF electrolyte (EC+EMC+LiPF$_6$+FEC), the outer layer with more organic components was found to be lithium alkyl carbonates, carboxylate, PEO oligomers, LEC and LEDC.[49,54,55] The inner layer with more inorganic components mainly consist of LiF and LiPF$_6$, with a small amount of Li$_2$CO$_3$ (**Figure 5b**).[56–58] In our studies, the SEI was porous and thin and was easily removed after DMC washing and ultrasonication. During calendar aging, this SEI was not thick or strong enough, and was unable to prevent silicon core from the corrosion of electrolytes, leading to inferior calendar life. The use of GenFM electrolyte (**Figure 5c**) most likely resulted in a similar SEI morphology and composition. Some of Mg ions reacted with electrolytes and surface oxide, forming MgF$_2$ and MgO in the inner layer. Based on the thermodynamic calculation, MgO probably transformed to MgF$_2$ (**Table S5**). Mg ions also diffused into the silicon core, forming the Li-Si-Mg ternary Zintl phase and reduced the content of Mg ions in the electrolyte and SEI leading to relatively porous and

thin SEI which also could not fully protect the silicon core from side reactions. For silicon electrodes in GenFC electrolyte, due to the slow diffusion of Ca^{2+} into silicon anode, most of the Ca ions were aggregated around silicon particles. During the lithiation, as the potential on the anode decreases, $LiPF_6$, FEC, and TFSI decomposition lead to F ion formation.[59–61] The F ions and Ca ions presumably rigorously reacts because of the low formation energy of CaF_2, leading to the formation of a strong CaF_2 in the SEI inner layer (**Figure 5d**). The sharp peak near 60 ppm in ^{13}C NMR spectra of indicated possible trapped solvents inside the SEIs (**Figure 4b**), suggesting that the SEIs in the GenF and GenFM samples were porous whereas SEI in GenFC is more nonporous as no solvent peak was observed with 13C NMR. Due to the high stability and less porosity of CaF_2, this inner layer shielded the silicon core during calendar aging, leading to better calendar life performance. The Ca additive may also alter the organic species in the SEIs. According to the SEM EDS and NMR characterizations, the Si electrodes in the GenF cells exhibited the most build-up of organic species while the Si electrodes in the GenFC cells showed the least. It is possible that Ca ions promoted the decomposition of fluorine bearing compounds, leading to more inorganic fluorides and less organic species. Worth mentioning is that in general the capacity decay of batteries during calendar aging is contributed by the degradation of both electrodes and electrolytes. However, in this study, the amount of electrolyte is excessive. CaF_2 in SEI layer and ternary Zintl phases formed can further stabilize interfaces,[44,62] leading to fewer electrolyte reactions. Therefore, it is safe to believe that most of the capacity decay is due to the electrode materials.

25

One important takeaway is that the requirement of SEI for long calendar life may differ from the one for long cycling life. For stable cycling, a flexible and relatively thin SEI that can flex with the volume change is superior as it consumes fewer electrolytes/silicon during the repeated formation and has lower interfacial impendence. For long calendar life, a nonporous and strong SEI that can prevent electrolyte infiltration and current leakage is advantageous. However, when cycling, such thick and hard SEI may interfere with the ion transfer, leading to relatively lower initial capacity and slightly inferior rate performance (**Figure S2**); it may also fracture while deforming, leading to extra consumption of electrolytes. Therefore, when designing practical silicon electrodes with long cycling life, high capacity retention rate, and long calendar life, a compromise and balance between each property may need to be considered which is the focus of a follow-up study, indicating a future path for the optimization of SEI compositions and structures.
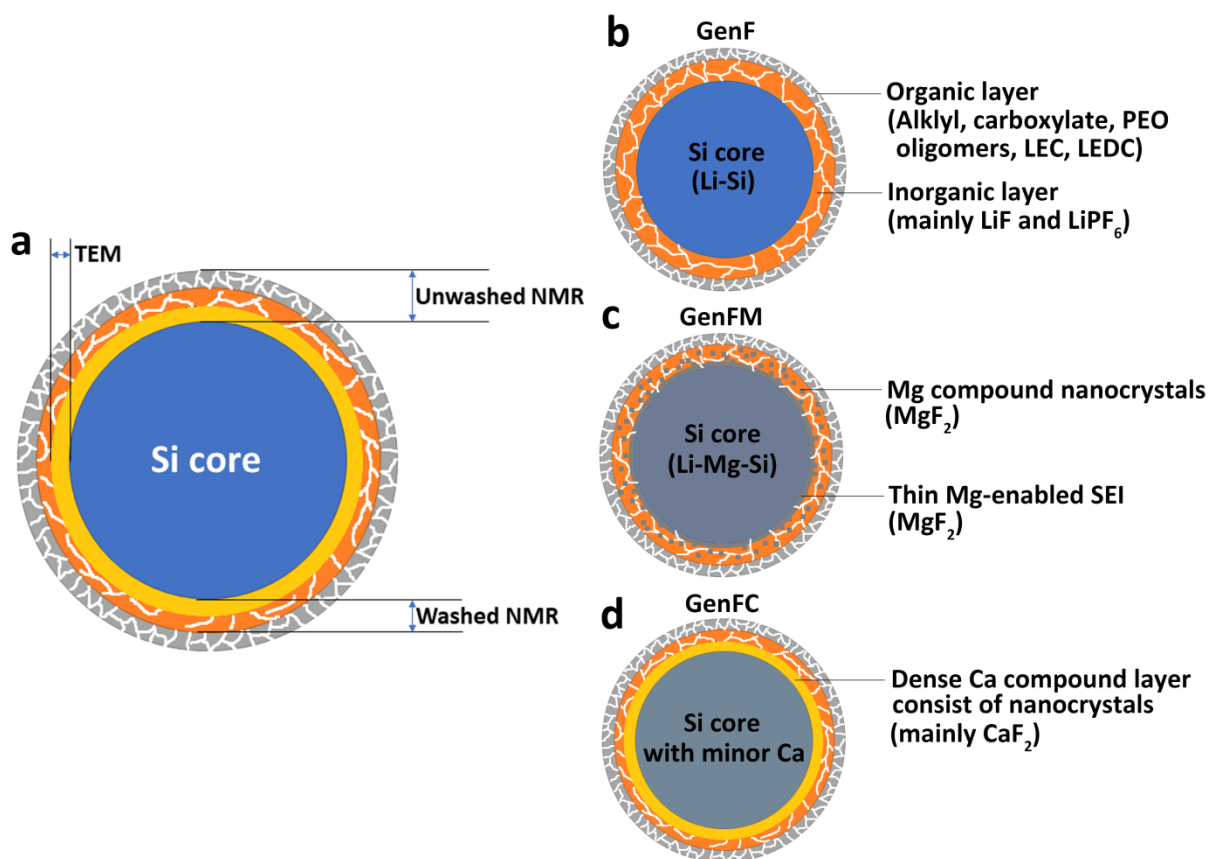
Figure 5. Schematic illustration of SEIs in GenF, GenFM, and GenFC cells. a) Schematic illustration of a silicon particle with multi-layered SEI after calendar aging and the information we derived from TEM and NMR characterizations. b)-d) Schematic illustration of SEIs in GenF, GenFM, and GenFC cells.

4. Conclusion

The study provides a viable approach to improve the calendar life of silicon electrodes regardless of the silicon anode source and type of cathode used, by adding a small concentration of Ca salts as an additive into the electrolyte. The addition of Ca^{+2} not only stabilizes silicon anions via the formation of Li-Ca-Si ternary phases electrochemically, but also rigorously reacts with F ions in the electrolyte forming a thick, robust and dense CaF_2 containing inorganic SEI around silicon particles. TEM characterizations validated that this CaF_2 layer had a thickness around 100 nm and consisted of nanocrystals embedded in an

amorphous matrix. It is strong enough to survive severe ultrasonication washing. Solid state NMR studies on both washed and unwashed samples unveiled that the Ca additive led to more inorganic compounds in the SEI, such as LiF and CaF_2 as well as the formation of poly-FEC. Because of the high stability of CaF_2 as well as other inorganic compounds, the new SEI is more stable and able to protect the silicon core from side reactions more effectively during calendar aging. On average, the Si/NMC532/GenFC cells lost 6.98 % of capacity after three-month calendar aging at 4.1 V, which is much better than GenF cells (13.71 %) and GenFM cells (14.86 %). More importantly, the improvement of the calendar life due to the Ca additive is universal and occurred in all tested commercial silicon or SiO sources with different cathodes. The multivalent Ca additives provide a new pathway towards practical high silicon content electrodes with long calendar life and long cycling life. We hope that our results inspire the field to work on surface stabilization for improved calendar life in silicon anodes through the application of CaF_2 coating and other coatings as well.

5. Experimental Section

Materials and electrodes preparation: The graphite-free Si electrodes were prepared by laminating the Cu foil as the current collector with a slurry containing 60 wt. % commercial silicon powders from Paraclete or Sigma-Aldrich, 20 wt. % hard carbon additive (C45), and 20 wt. % lithium polyacrylate (LiPAA) silicon compatible binder, mixed in deionized water. The Si electrode has a final loading of 0.63 mg/cm^2. Other electrodes were provided

by Argonne's Cell Analysis, Modeling, and Prototyping (CAMP) facility. Specifically, the NMC532 electrodes were made of 90 wt % $LiNi_{0.5}Mn_{0.3}Co_{0.2}O_2$ from Toda, 5 wt. % C45, and 5 wt. % poly(vinylidene fluoride) (PVDF) binder, with a loading of 8.98 mg/cm^2; the LFP electrodes were made of 90 wt. % $LiFePO_4$ from Johnson Matthey, 5 wt. % C45, and 5 wt. % poly(vinylidene fluoride) (PVDF) binder, with a loading of 19.70 mg/cm^2; the SiO electrodes were made of 70 wt. % SiO from Osaka, 10 wt. % C45, and 20 wt. % P84 Polyimide (PI) binder, with a loading of 1.72 mg/cm^2. All the electrodes were dried in the vacuum oven at 150 °C for 8 hours before use.

Coin cell assembling and test: In this work, 2032-type coin cells were used to test the electrochemical performance. In the full-cell tests, the negative electrodes were Si or SiO, and the positive electrodes were NMC532 or LFP cathodes. The separators were Celgard-2320. Various electrolyte formulations were used in this study, with their compositions listed in **Table 1**. $Mg(TFSI)_2$ and $Ca(TFSI)_2$ with a purity of 99.5 % were bought from Solvionic and dried in the vacuum oven at 160 °C before use. The typical full cell calendar life test starts from a 4-hour open circuit voltage rest. Subsequently, there are three formation cycles at a C/10 rate in the voltage window of 3.0 to 4.1 V for NMC532 and 2.7 to 3.35 V for LFP followed by a one-month or three-month holding at 4.1 V or 3.35 V. Finally, there are two diagnostic cycles at C/10 rate. The cyclic performance of Si/NMC532 full cells is tested at a C/10 rate for 100 cycles. Electrochemical impedance spectroscopy (EIS) tests in the frequency range from 100 kHz to 0.001 Hz with an AC perturbation of 5

mV were carried out using a CHI 660E electrochemical workstation. Batteries for EIS tests are at a fully discharged state with a voltage around 3.0 V. The analysis of EIS spectra is done on a free software EIS Spectrum Analyser developed by A. S. Bondarenko and G. A. Ragoisha.

Material Characterization:

^{1}H, ^{13}C, and ^{19}F MAS NMR experiments were performed at 11.74 T (500 MHz) on a Bruker Avance III HD spectrometer operating at a Larmor frequency of 125.76 and 470.49, respectively. A rotor synchronized echo pulse sequence ($\pi/2$ - τ -π - acq.), where $\tau= 1/\nu_r$ (spinning frequency), was used to acquire the ^{19}F MAS NMR spectra with a 1.3 mm probe at a spinning speed of 50 kHz with a pulse width of 1.8 µs and a pulse delay of 5s. ^{19}F chemical shifts are given relative to CCl_3F, referenced using a secondary reference of LiF at 204ppm. ^{1}H/^{13}C Cross Polarization experiments were used to acquire ^{13}C NMR data on a 1.3 mm probe with a 20kHz spinning speed. A contact time of 4 ms and pulse delay of 2 s were used. The spectra were referenced to TMS at 0 ppm. Scanning electron microscopy (SEM) studies were performed at 20 kV on an FEI Quanta 400F ESEM in the Center for Nanoscale Materials at Argonne National Laboratory. TEM studies were performed at 200 kV on an FEI Talos F200X TEM/STEM in the Center for Nanoscale Materials at Argonne National Laboratory. This TEM is equipped with a Super X energy-dispersive spectrometer (EDS) from Bruker. The TEM samples were prepared by washing and sonicating the post-

electrochemical-test Si electrode in dimethyl carbonate (DMC) and then drop cast onto Cu grids with lacey carbon films in a glovebox.

Density functional theory (DFT) calculation: Predicted solid state reaction enthalpies were obtained using the reaction calculator module in pymatgen.[63,64] DFT optimized structures and total energies were obtained from the Materials Project,[50] a database of density functional theory calculations. These calculations are performed at 0 K and 0 bar and do not take entropy into consideration, this can introduce error in two manners. First, the calculated enthalpies for individual polymorphs may differ from experimental enthalpies, however, reasonable agreement is found between experimental and calculated formation enthalpies. Second, the predicted lowest-energy DFT phase may not match the experimentally observed phase.

Supporting Information

Supporting Information is available from the Wiley Online Library or from the author.

Conflict of Interest

The authors declare no conflict of interest.

Data Availability Statement

The data that support the findings of this study are available on request from the corresponding author.

References

[1]   A. M. Andwari, A. Pesiridis, S. Rajoo, R. Martinez-Botas, V. Esfahanian, *Renew. Sustain. Energy Rev.* **2017**, *78*, 414.

[2]   W. Li, E. M. Erickson, A. Manthiram, *Nat. Energy* **2020**, *12*, 26.

[3]   J. Shi, D. Xiao, M. Ge, X. Yu, Y. Chu, X. Huang, X. Zhang, Y. Yin, X. Yang, Y. Guo, L. Gu, L. Wan, *Adv. Mater.* **2018**, *30*, 1705575.

[4]   X. Zeng, C. Zhan, J. Lu, K. Amine, *Chem* **2018**, 690.

[5]   K. Wang, J. Wan, Y. Xiang, J. Zhu, Q. Leng, M. Wang, L. Xu, Y. Yang, *J. Power Sources* **2020**, *460*, 228062.

[6]   J. Liu, Z. Bao, Y. Cui, E. J. Dufek, J. B. Goodenough, P. Khalifah, Q. Li, B. Y. Liaw, P. Liu, A. Manthiram, Y. S. Meng, V. R. Subramanian, M. F. Toney, V. V Viswanathan, M. S. Whittingham, J. Xiao, W. Xu, J. Yang, X. Yang, J. Zhang, *Nat. Energy* **2019**, *4*, 180.

[7]   J. W. Choi, D. Aurbach, *Nat. Rev. Mater.* **2016**, *1*, 16013.

[8]   U. Kasavajjula, C. Wang, A. J. Appleby, *J. Power Sources* **2007**, *163*, 1003.

[9]   J. P. Maranchi, S. L. A, J. P. Maranchi, A. F. Hepp, P. N. Kumta, *Electrochem. Solid-State Lett.* **2003**, *6*, A198.

[10] H. Wu, Y. Cui, *Nano Today* **2012**, *7*, 414.

[11] Y. Zhang, F. M. Heim, N. Song, J. L. Bartlett, X. Li, *ACS Energy Lett.* **2017**, 2696.

[12] C. Fang, X. Wang, Y. S. Meng, *Trends Chem.* **2019**, *1*, 152.

[13] Y. H. Xu, G. P. Yin, P. J. Zuo, *Electrochim. Acta* **2008**, *54*, 341.

[14] S. Lee, J. Lee, S. Chung, H. Lee, S. Lee, H. Baik, *J. Power Sources* **2001**, *97–98*, 191.

[15] M. Gu, Y. Li, X. Li, S. Hu, X. Zhang, W. Xu, S. Thevuthasan, D. R. Baer, J.-G. Zhang, J. Liu, C. Wang, *ACS Nano* **2012**, *6*, 8439.

[16] P. Hovington, M. Dontigny, A. Guer, J. Trottier, M. Lagacé, A. Mauger, C. M. Julien, K. Zaghib, *J. Power Sources* **2014**, *248*, 457.

[17] Z. Ma, T. Li, Y. L. Huang, J. Liu, Y. Zhou, D. Xue, *RSC Adv.* **2013**, *3*, 7398.

[18] J. Wang, X. Wang, B. Liu, H. Lu, G. Chu, J. Liu, Y. Guo, X. Yu, F. Luo, Y. Ren, L. Chen, H. Li, *Nano Energy* **2020**, *78*, 105101.

[19] M. Ashuri, Q. He, L. L. Shaw, *Nanoscale* **2016**, *8*, 74.

[20] J. R. Szczech, S. Jin, *Energy Environ. Sci.* **2011**, *4*, 56.

[21] G. M. Carroll, M. C. Schulze, T. R. Martin, G. F. Pach, J. E. Coyle, G. Teeter, N. R. Neale, *ACS Appl. Energy Mater.* **2020**, *3*, 10993.

[22] C. K. Chan, H. Peng, G. Liu, K. McIlwrath, X. F. Zhang, R. a Huggins, Y. Cui, *Nat. Nanotechnol.* **2008**, *3*, 31.

[23] M. Park, M. G. Kim, J. Joo, K. Kim, J. Kim, S. Ahn, Y. Cui, J. Cho, *Nano Lett.* **2009**, *9*, 3844.

[24] F. Dogan, L. D. Sanjeewa, S. Hwu, J. T. Vaughey, *Solid State Ionics* **2016**, *288*, 204.

[25]   M. Salah, P. Murphy, C. Hall, C. Francis, R. Kerr, M. Fabretto, *J. Power Sources* **2019**, *414*, 48.

[26]   Y. Yao, M. T. Mcdowell, I. Ryu, H. Wu, N. Liu, L. Hu, W. D. Nix, Y. Cui, *Nano Lett.* **2011**, *11*, 2949.

[27]   G. Wang, Z. Wen, Y. Yang, J. Yin, W. Kong, S. Li, J. Sun, S. Ji, *J. Mater. Chem. A* **2018**, *6*, 7557.

[28]   M. V Shelke, H. Gullapalli, K. Kalaga, M. F. Rodrigues, R. R. Devarapalli, R. Vajtai, P. M. Ajayan, *Adv. Mater. Interfaces* **2017**, *4*, 1601043.

[29]   A. Barré, F. Suard, M. Gérard, M. Montaru, D. Riu, *J. Power Sources* **2014**, *245*, 846.

[30]   J. D. Mcbrayer, M. F. Rodrigues, M. C. Schulze, P. Daniel, C. A. Apblett, I. Bloom, G. M. Carroll, A. M. Colclasure, C. Fang, K. L. Harrison, G. Liu, S. D. Minteer, N. R. Neale, A. K. Burrell, B. Cunningham, *Nature Energy*, **2021**, Accepted for publication**.**

[31]   APPENDIX A – Lithium Electrode Based Cell Goals, *USABC* **2021**.

[32]   J. Danet, T. Brousse, K. Rasim, P. Moreau, *Phys. Chem. Chem. Phys.* **2010**, *12*, 220.

[33]   B. Key, R. Bhattacharyya, M. Morcrette, V. Sezne, J. Tarascon, C. P. Grey, D. P. J. Verne, *J. Am. Chem. Soc.* **2009**, *131*, 9239.

[34]   B. Key, M. Morcrette, J. Tarascon, C. P. Grey, *J. Am. Chem. Soc.* **2011**, *133*, 503.

[35]   M. Nie, D. P. Abraham, Y. Chen, A. Bose, B. L. Lucht, *J. Phys. Chem. C* **2013**, *117*, 13403.

[36]   J. Cho, S. T. Picraux, *Nano Lett.* **2014**, 3088.

[37]   Y. Yin, E. Arca, L. Wang, G. Yang, M. Schnabel, L. Cao, C. Xiao, H. Zhou, P. Liu, J.

Nanda, G. Teeter, B. Eichhorn, K. Xu, A. Burrell, C. Ban, *ACS Appl. Mater. Interfaces* **2020**, *12*, 26593.

[38]　E. Peled, S. Menkin, *J. ofThe Electrochem. Soc.* **2017**, *164*, A1703.

[39]　K. Kalaga, M. F. Rodrigues, S. E. Trask, I. A. Shkrob, D. P. Abraham, *Electrochim. Acta* **2018**, *280*, 221.

[40]　I. Zilberman, J. Sturm, A. Jossen, *J. Power Sources* **2019**, *425*, 217.

[41]　W. Lu, J. E. Soc, W. Lu, Y. Qin, A. Jansen, *J. Electrochem. Soc.* **2018**, *165*, A2179.

[42]　V. Baran, L. Van Wüllen, T. F. Fässler, *Chem. Eur. J.* **2016**, *22*, 6598.

[43]　M. Zeilinger, V. Baran, L. van Wüllen, U. Häussermann, T. F. Fässler, *Chem. Mater.* **2013**, *25*, 4113.

[44]　B. Han, C. Liao, F. Dogan, S. E. Trask, S. H. Lapidus, J. T. Vaughey, B. Key, *ACS Appl. Mater. Interfaces* **2019**, *11*, 29780.

[45]　M. Schulze, M. T. F. Rodrigues, J. McBrayer, I. Bloom, A. Colclasure, D. Abraham, G. Veith, N. Neale, A. Burrell, J. Vaughey, C. Johnson, Silicon Consortium Project Calendar Aging Electrochemical Screening Protocol 1.2. **2021**, https://www.nrel.gov/transportation/silicon-anode-consortium.html.

[46]　F. Single, A. Latz, B. Horstmann, *ChemSusChem* **2018**, *11*, 1950.

[47]　B. Gyenes, J. E. Soc, B. Gyenes, D. A. Stevens, V. L. Chevrier, J. R. Dahn, *J. Electrochem. Soc.* **2015**, *162*, A278.

[48]　S. Seidlmayer, P. Keil, R. Gilles, A. Jossen, *J. Power Sources* **2017**, *365*, 327.

[49]　A. L. Michan, M. Leskes, C. P. Grey, *Chem. Mater.* **2016**, *28*, 385.

[50] A. Jain, S. P. Ong, G. Hautier, W. Chen, W. D. Richards, S. Dacek, D. Gunter, D. Skinner, G. Ceder, K. A. Persson, A. Jain, P. Ong, G. Hautier, W. Chen, D. Gunter, D. Skinner, G. Ceder, K. A. Persson, *APL Mater.* **2013**, *1*, 011002.

[51] M. Spoliti, L. Bencivenni, F. Ramondo, V. Rossi, *J. Mol. Struct.* **1994**, *315*, 19.

[52] Y. Zhang, N. Du, D. Yang, *Nanoscale* **2019**, *11*, 19086.

[53] A. Wang, S. Kadam, H. Li, S. Shi, Y. Qi, *npj Comput. Mater.* **2018**, *4*, 15.

[54] C. K. Chan, R. Ruffo, S. Sae, Y. Cui, *J. Power Sources J.* **2009**, *189*, 1132.

[55] A. L. Michan, G. Divitini, A. J. Pell, M. Leskes, C. Ducati, C. P. Grey, *J. Am. Chem. Soc.* **2016**, *138*, 7918.

[56] Q. Li, X. Liu, X. Han, Y. Xiang, G. Zhong, J. Wang, B. Zheng, J. Zhou, Y. Yang, *ACS Appl. Mater. Interfaces* **2019**, *11*, 14066.

[57] Y. Jin, N.-J. H. Kneusels, L. E. Marbella, E. Castillo-Martínez, P. C. M. M. Magusin, R. S. Weatherup, E. Jónsson, T. Liu, S. Paul, C. P. Grey, *J. Am. Chem. Soc.* **2018**, *140,* 9854.

[58] M. Sina, J. Alvarado, H. Shobukawa, C. Alexander, V. Manichev, L. Feldman, T. Gustafsson, K. J. Stevenson, Y. S. Meng, *Adv. Energy Mater.* **2016**, *3*, 1600438.

[59] A. Guéguen, J. E. Soc, D. Streich, M. He, M. Mendez, F. F. Chesneau, P. Nov, E. J. Berg, *J. ofThe Electrochem. Soc.* **2016**, *163*, A1095.

[60] R. Jung, J. E. Soc, R. Jung, M. Metzger, D. Haering, S. Solchenbach, C. Marino, N. Tsiouvaras, C. Stinner, H. A. Gasteiger, *J. Electrochem. Soc.* **2016**, *163*, A1705.

[61] Z. Xu, J. Yang, H. Li, Y. Nuli, J. Wang, *J. Mater. Chem. A* **2019**, *7*, 9432.

[62] X. Li, J. A. Gilbert, S. E. Trask, R. Uppuluri, S. H. Lapidus, S. Cora, N. Sa, Z. Yang, I. D. Bloom, F. Dogan, J. T. Vaughey, B. Key, *Chem. Mater.* **2021**, *33*, 4960.

[63] A. Jain, G. Hautier, S. P. Ong, C. J. Moore, C. C. Fischer, K. A. Persson, G. Ceder, *Phys. Rev. B* **2011**, *84*, 045115.

[64] S. Ping, W. Davidson, A. Jain, G. Hautier, M. Kocher, S. Cholia, D. Gunter, V. L. Chevrier, K. A. Persson, G. Ceder, *Comput. Mater. Sci.* **2013**, *68*, 314.